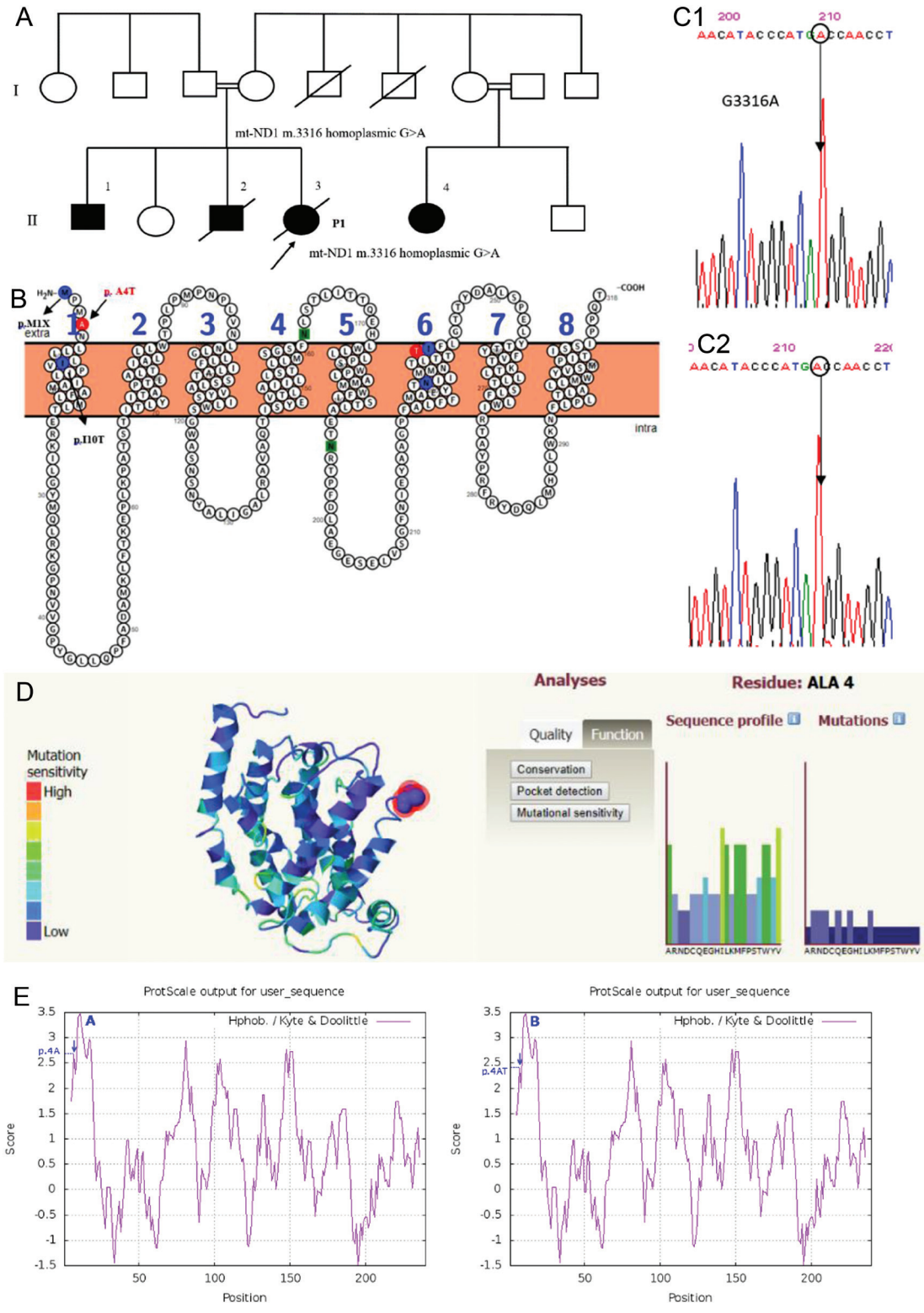


Supplementary FIG. 1. Pedigree of patient (P)1 (A), prediction of transmembrane structures of the wild-type mitochondrial ND1 protein performed by Protter program (B), Sanger sequencing data showing the m.3316 G>A, change in the *MT-ND1* gene in patient (C1), Sanger sequencing data showing the m.3316 G>A, change in the *MT-ND1* gene in patients' mother (C2), prediction of tertiary structure models and possible effect of position change for p.A4T by Phyre2 server (D), a hydropathy plot evaluated in ExPASy-ProtScale program Kyte-Doolittle algorithm for the ND1 protein. The hydrophobicity of the wild-type ND1 protein [control (A)] is compared to the variant forms (B) and (E).

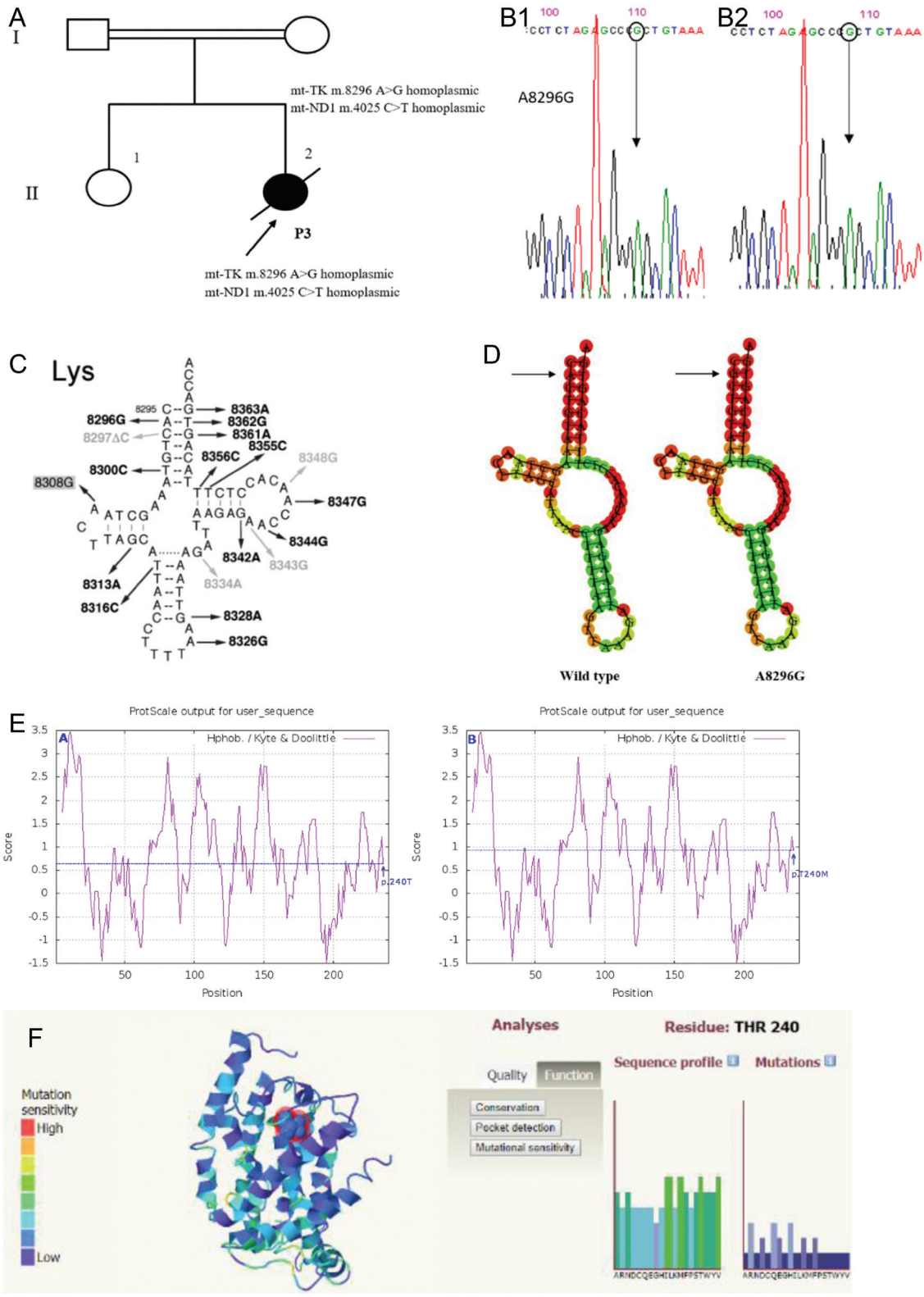


Supplementary FIG. 2. Pedigree of P3 (A), Sanger sequencing data showing the m.8296 A>G, change in the tRNA-Lysine gene in patient (B1) and mother (B2), secondary structure of mt-TK (grey dots show polymorphism and black dots show pathogenic regions) (C), predicted secondary structure of wild type (left) and mutant A8296G (right) tRNA-Lysine evaluated in RNA fold web server (D), predicted tertiary structure models and possible effect of position change for p.T240M by Phyre2 server in P3 (E), a hydropathy plot evaluated in ExPASy-ProtScale program Kyte-Doolittle algorithm for the ND1 protein. The hydrophobicity of the wild-type ND1 protein (control- (A)) is compared to the variant forms (B) and (F).

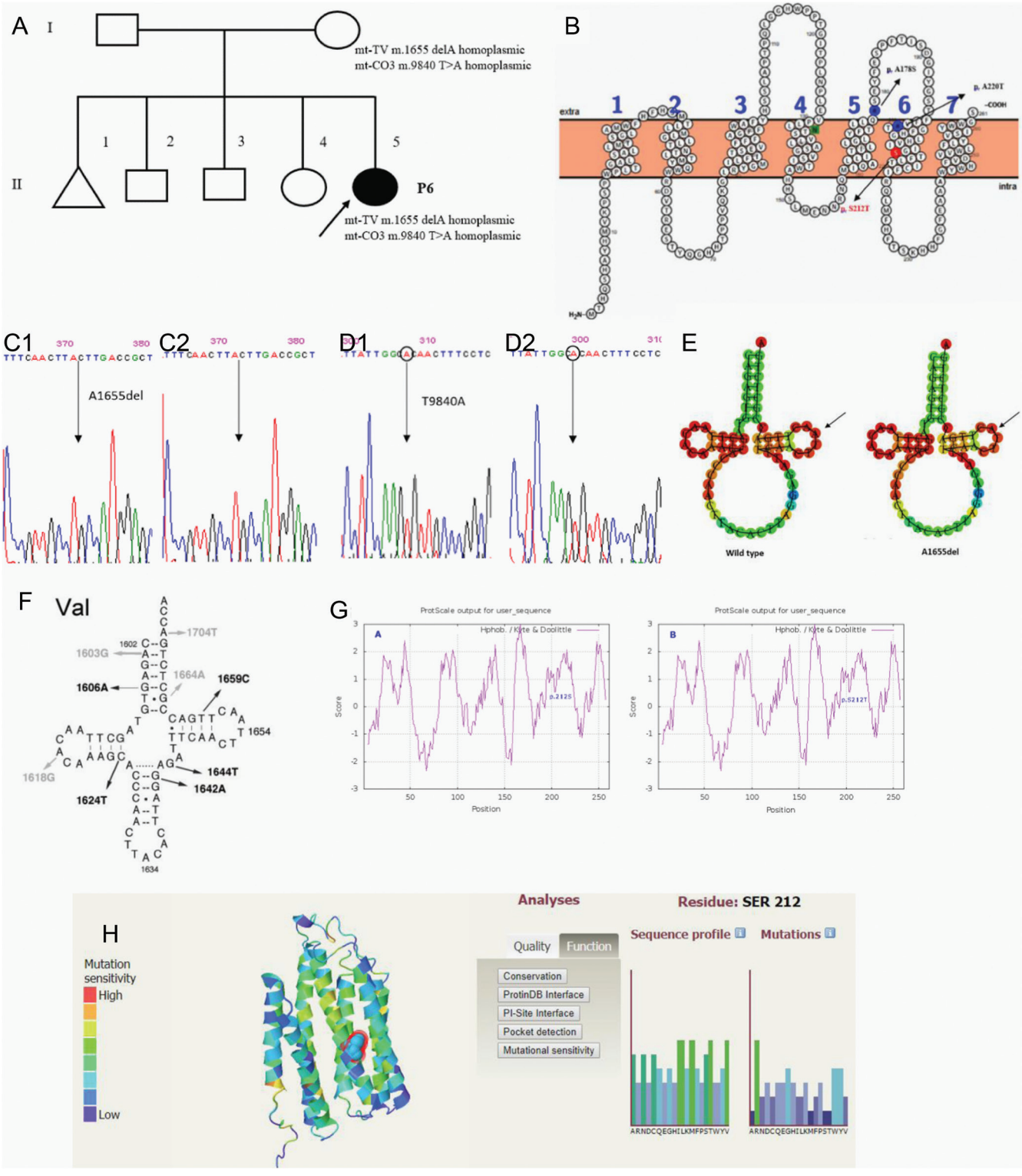


Supplementary FIG. 3. Pedigree of P6 (A), prediction of transmembrane structures of the wild-type mitochondrial CO3 protein performed by Protter program (B), Sanger sequencing data showing the m.1655 delA change in the tRNA-Val gene in patient (C1) and mothers (C2), Sanger sequencing data showing the m.9840 T>A change in the *mt-CO3* gene in patient (D1) and mother (D2), predicted secondary structure of wild type (left) and mutant A1655del (right) tRNA-Lysine evaluated in RNA fold web server (E), secondary structure of mt-TV (grey dots show polymorphism and black dots show pathogenic regions) (F), a hydropathy plot evaluated in ExPASy-ProtScale program Kyte-Doolittle algorithm for the CO3 protein. The hydrophobicity of the wild-type CO3 protein [control (A)] is compared to the variant forms (B) and (G), predicted tertiary structure models and possible effect of position change for p.S212T by Phyre2 server in P6 (H).

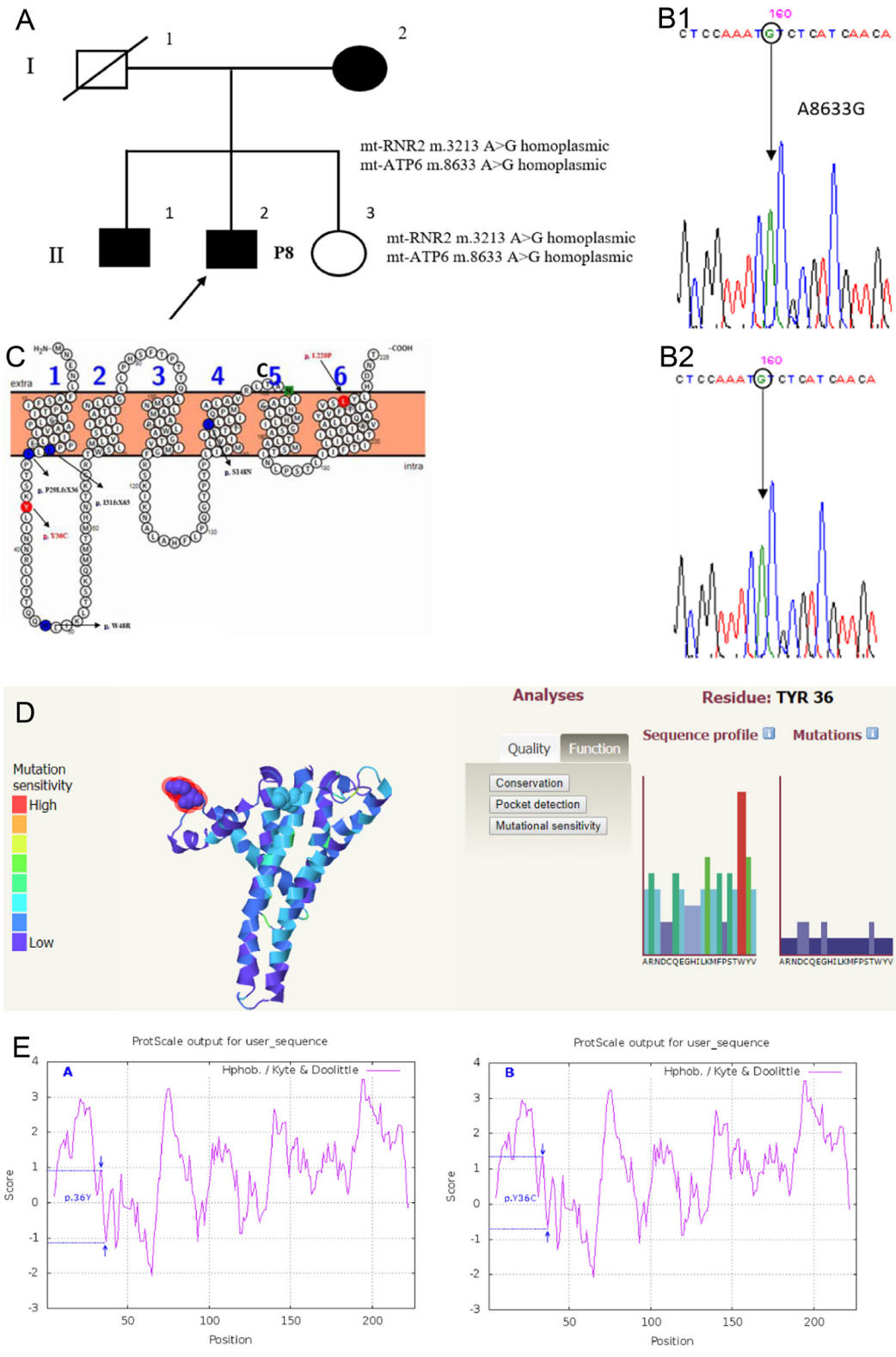


Supplementary FIG. 4. A-E. Pedigree of P8 (A), Sanger sequencing data showing the m.8633 A>G change in the mt-ATP6 gene in patient (B1) and mother (B2), prediction of transmembrane structures of the wild-type mitochondrial ATP6 protein performed by Protter program (C), prediction of tertiary structure models and possible effect of position change for p.Y36C by Phyre2 server in P9 (D), a hydropathy plot evaluated in ExPASy-ProtScale program Kyte-Doolittle algorithm for the ATP6 protein. The hydrophobicity of the wild-type ATP6 protein (control- (A)) is compared to the variant forms (B) and (E).

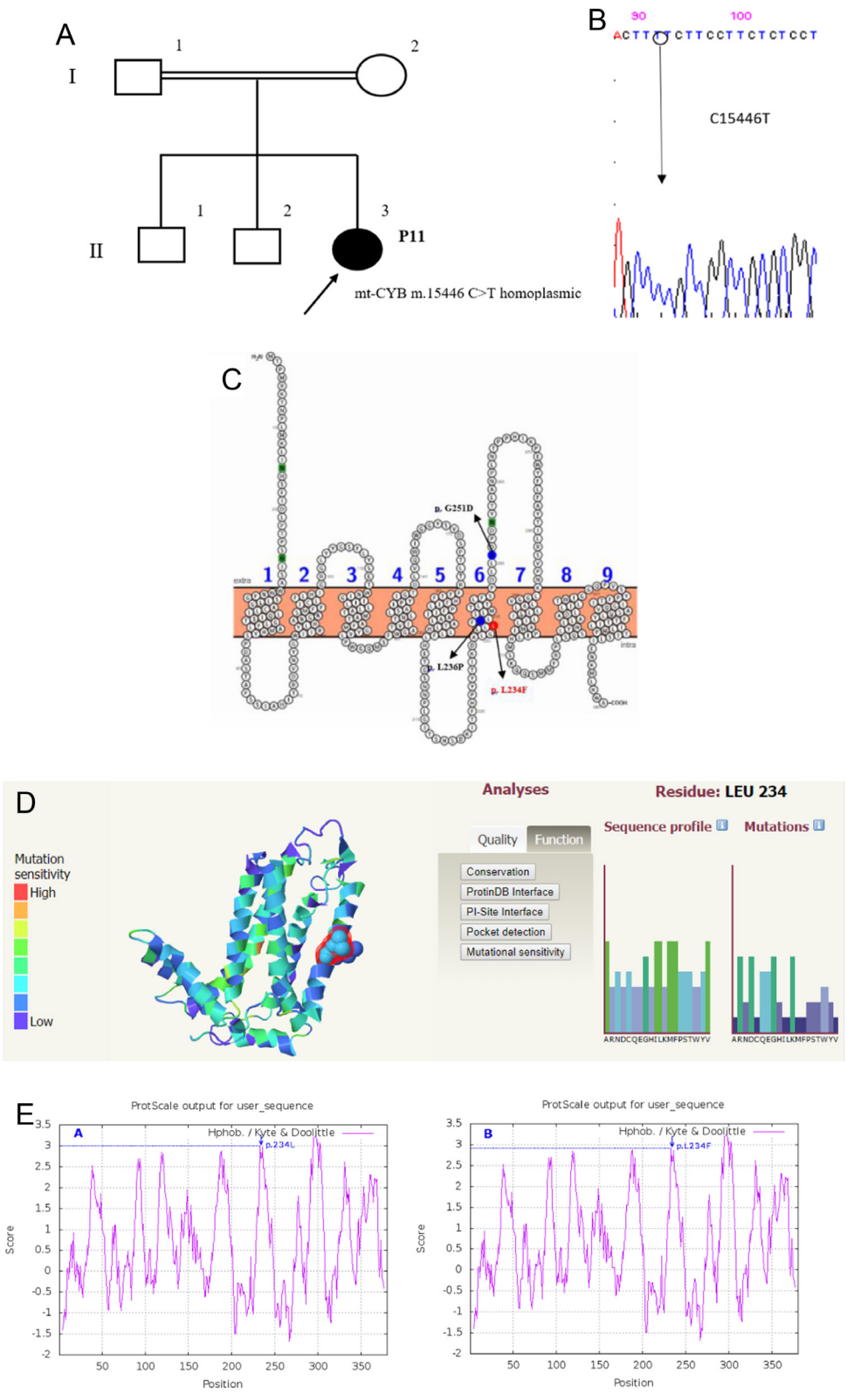


Supplementary FIG. 5. A-E. Pedigree of P11 (A), Sanger sequencing data showing the m.15446 C>T change in the mt-CYB gene (B), prediction of transmembrane structures of the wild-type mitochondrial CYB protein performed by Protter program (C), prediction of tertiary structure models and possible effect of position change for p.L234F by Phyre2 server in P12 (D), a hydropathy plot evaluated in ExPASy-ProtScale program Kyte-Doolittle algoritm for the CYB protein. The hydrophobicity of the wild-type CYB protein (control (A) is compared to the variant forms (B) and (E).

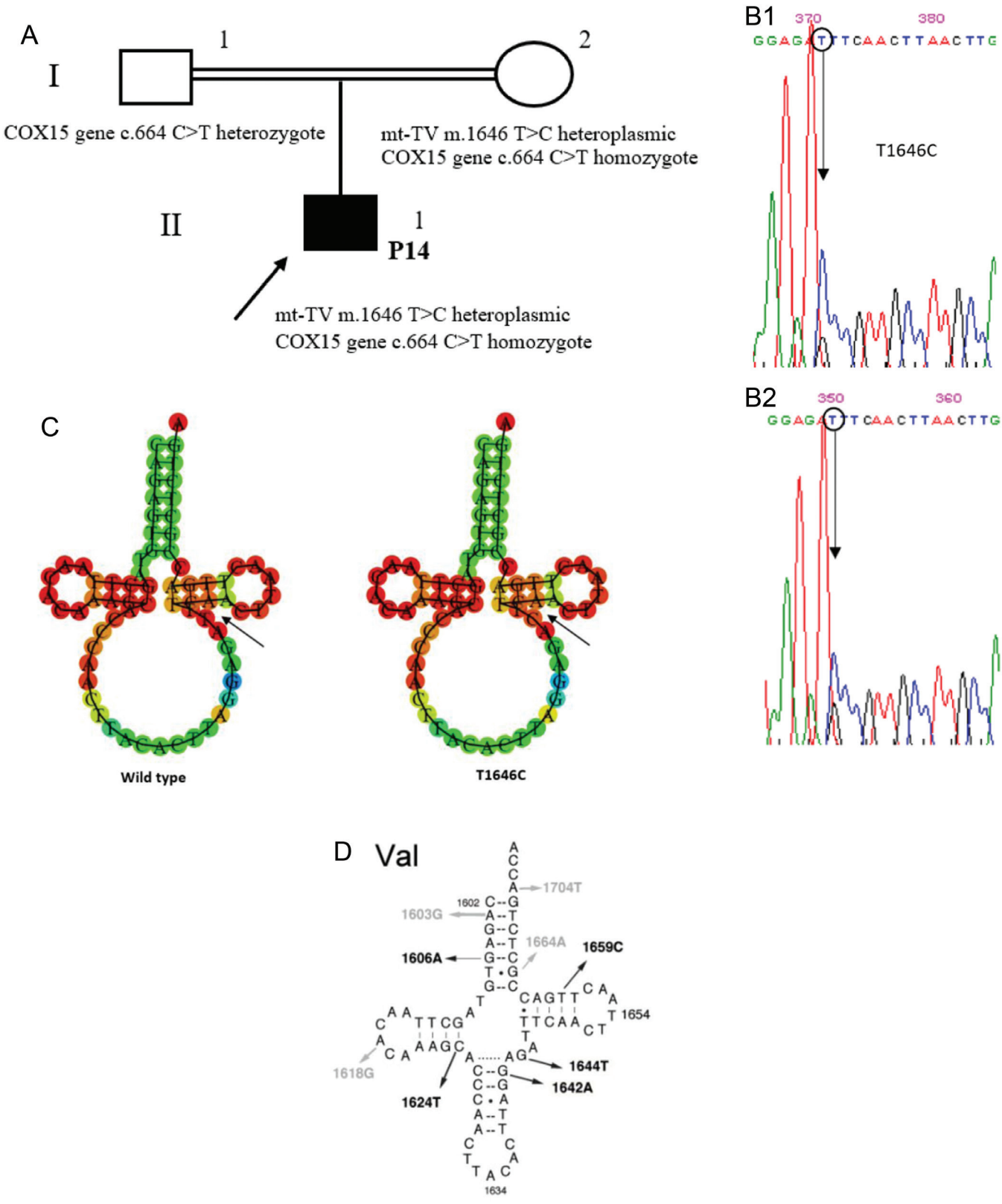


Supplementary FIG. 6. A-D. Pedigree of P14 (A), Sanger sequencing data showing the m.1646 T>C change in the tRNA-Val gene in patient (B1) and mother (B2), predicted secondary structure of wild type (left) and mutant T1646C (right) tRNA-Val evaluated in RNA fold web server (C), secondary structure of mt-TV (grey dots show polymorphism and black dots show pathogenic regions) (D).